Earth and Planetary Science Letters 616 (2023) 118211

Contents lists available at ScienceDirect

Earth and Planetary Science Letters

journal homepage: www.elsevier.com/locate/epsl

Highly fractionated Hg isotope evidence for dynamic euxinia in shallow waters of the Mesoproterozoic ocean

Yaowen Wu [a,b], Hui Tian [a,b,*], Runsheng Yin [c], Di Chen [c], Stephen E. Grasby [d], Jun Shen [e], Tengfei Li [a,b], Sui Ji [a,b], Ping'an Peng [a,b]

[a] State Key Laboratory of Organic Geochemistry, Guangzhou Institute of Geochemistry, Chinese Academy of Sciences, Guangzhou 510640, China
[b] CAS Center for Excellence in Deep Earth Science, Guangzhou 510640, China
[c] State Key Laboratory of Ore Deposit Geochemistry, Institute of Geochemistry, Chinese Academy of Sciences, Guiyang 550081, China
[d] Geological Survey of Canada, Natural Resources Canada, 3303 33rd Street NW, Calgary, Alberta T2L 2A7, Canada
[e] State Key Laboratory of Geological Processes and Mineral Resources, China University of Geosciences, Wuhan, Hubei 430074, China

ARTICLE INFO

Article history:
Received 29 August 2022
Received in revised form 27 April 2023
Accepted 4 May 2023
Available online 31 May 2023
Editor: B. Wing

Keywords:
redox structure
photic zone euxinia
Mesoproterozoic
Hg isotope
eukaryote evolution

ABSTRACT

Studies of Mesoproterozoic ocean chemistry have converged on a widely accepted scenario where a stable shallow layer of oxic waters occurred over deeper anoxic ferruginous waters, with mid-depth euxinic waters restricted to continental margins. However, several lines of evidence suggest shallow waters may not always have remained oxic, but fluctuated between oxic, anoxic, and euxinic conditions. Here, we present new Hg-C-S geochemistry data of ca. 1.5–1.4 Ga sediments in the Yanliao Basin to better understand the redox structure of shallow water environments, especially for the photic zone. In this study, positive Δ^{199}Hg values suggest atmospheric Hg(II) deposition into oxic surface waters, whereas abnormally negative Δ^{199}Hg values indicate enhanced sequestration of gaseous Hg(0) and photo-reduction of reduced sulfur-bound Hg(II) in response to photic zone euxinia. Our highly fractionated Δ^{199}Hg values reveal a new scenario, in which the extent of euxinia is more dynamic than generally thought, and may expand from the mid-depth to the photic zone, likely linked to the superimposed operation of enhanced oxidative weathering input of SO_4^{2-} and high OM flux in the water column. Given that euxinic waters may accelerate the sequestration of bio-essential elements, it is suggested that the dynamic euxinia of shallow water played a significant role in delaying the diversification of eukaryotes in the Mesoproterozoic oceans. Our study also highlights that Hg isotopes may act as a promising new proxy to trace redox changes in the surface ocean over geological time.

1. Introduction

Protracted oxygenation of Earth's atmosphere and ocean systems significantly influenced the evolution of early life (e.g., Lyons et al., 2014). It is widely accepted that the Archean ocean–atmosphere system (>2500 Ma) was dominantly reduced, except for some local oxygen oases (Anbar et al., 2007; Eickmann et al., 2018), whereas the Phanerozoic surface environment (< 541 Ma) was well-oxygenated and coincided with animal radiation (e.g., Knoll and Carroll, 1999). In contrast, the oxygen levels and marine redox structure of the transitional Proterozoic Eon, a critical period of diversification of early eukaryotes, have long been debated (e.g., Canfield, 1998; Poulton et al., 2010; Planavsky et al., 2011; Luo et al., 2014; Zhang et al., 2016, 2018).

The Mesoproterozoic Era (1600–1000 Ma) was a period of significant changes in ocean chemistry and the diversification of early eukaryotes (Planavsky et al., 2011; Zhang et al., 2016, 2018). The Mesoproterozoic oceans are thought to have been characterized by widespread euxinic (H_2S-rich) waters, following the disappearance of banded iron formations ca.1800 Ma ago (Canfield, 1998). Subsequent studies revealed a different scenario and suggested that the spatial occurrence of euxinia was confined to productive continental margins (e.g., Poulton and Canfield, 2011) and that deep waters still remained dominantly anoxic and ferruginous throughout most

* Corresponding author at: State Key Laboratory of Organic Geochemistry, Guangzhou Institute of Geochemistry, Chinese Academy of Sciences, Guangzhou 510640, China.
E-mail address: tianhui@gig.ac.cn (H. Tian).

https://doi.org/10.1016/j.epsl.2023.118211
0012-821X/

of the Mesoproterozoic (e.g., Planavsky et al., 2011; Poulton and Canfield, 2011). Recent investigations in different basins further indicate that the redox structure of Mesoproterozoic oceans may be more complex than previously thought, and that deep waters may have been episodically oxic (Sperling et al., 2014; Zhang et al., 2016; Planavsky et al., 2018). These contrasting results may reflect spatial and/or temporal redox heterogeneity of the Mesoproterozoic oceans, especially for the deep waters.

Despite the redox heterogeneity of deep waters, shallow waters were thought to be more or less oxic in the Mesoproterozoic oceans (e.g., Poulton and Canfield, 2011; Zhang et al., 2018). Using various proxies (e.g., Fe-S-C geochemistry data), some studies have provided evidence for a very shallow chemocline and/or episodic anoxia in shallow waters (Luo et al., 2014; Doyle et al., 2018). Moreover, several lines of evidence (organic biomarkers and Hg isotopes) also indicate episodic euxinia of surface waters in the Mesoproterozoic oceans (e.g., 1.1 Ga), probably in the photic zone (Brocks et al., 2005; Zheng et al., 2018). These results reveal that the redox conditions of shallow waters may also be spatially and temporally heterogeneous, probably due to low atmospheric oxygen levels (0.1–1% of present atmospheric levels (PAL); Planavsky et al., 2014). Eukaryotic fossils in the Mesoproterozoic were mainly confined to shallow environments (Javaux et al., 2001), and redox variations in shallow waters may have a specific significance for early eukaryotic diversification (Anbar and Knoll, 2002). Thus, more work is required to fully understand the links between the redox heterogeneity of shallow waters and the patterns of eukaryotic diversification in the Mesoproterozoic.

Fe speciation and trace metal redox proxies (e.g., Mo and U) have been widely used to trace redox variations among oxic, euxinic, anoxic and ferruginous conditions (e.g., Anbar and Knoll, 2002; Planavsky et al., 2011; Chen et al., 2020). These proxies provide valuable insights into the redox conditions of bottom or pore waters, but poor constraints on the redox information of surface waters, especially the photic zone. Particular organic biomarkers can provide evidence for photic zone euxinia due to anoxygenic photosynthesis via H_2S in the photic zone (e.g., Brocks et al., 2005), but some factors (e.g., contamination from artificial hydrocarbons and diagenetic alteration) may mislead the interpretations of organic biomarkers in Precambrian sediments (Brocks, 2011), and the absence of key biomarkers cannot be directly interpreted as the absence of photic zone euxinia. Mercury (Hg) isotopes, especially its mass-independent fractionation (Hg-MIF), have recently been exploited as a promising proxy to trace the redox changes in surface waters of Mesoproterozoic oceans (Zheng et al., 2018). This is because the photo-reduction of Hg(II) bound to oxygen-containing ligands and reduced sulfur ligands triggers positive and negative Hg-MIF in the residual Hg(II) of the water column, respectively, which is then inherited by sediments (Zheng et al., 2018).

A well preserved profile of sediments of the Yanliao Basin in the North China Craton records valuable information on redox changes in shallow waters of the Mesoproterozoic ocean (e.g., Luo et al., 2014; Zhang et al., 2016, 2018; Chen et al., 2020). The Fe speciation and trace metal data from 1.5–1.4 Ga sediments of the Yanliao Basin indicate fluctuating oxic or ferruginous bottom water conditions with intermittently euxinic bottom waters (Luo et al., 2014; Chen et al., 2020). Although the key biomarkers for anoxygenic phototrophs could constrain the redox changes in the photic zone, they were not identified in the 1.5–1.4 Ga sediments of the Yanliao Basin (Luo et al., 2016). Here, we test Hg isotope as a new proxy to understand the redox information of the photic zone. By combining published Fe speciation and trace metal data, we present new Hg-C-S geochemistry data from ca. 1.5–1.4 Ga sediments of the Yanliao Basin to provide new insights into the redox structure in shallow waters at the time and its implications for early eukaryotes evolution.

2. Background

2.1. Hg geochemistry cycling

Mercury concentrations and isotope composition have been recently used as robust proxies to recognize large volcanism and understand changes in ocean/atmospheric chemistry as well as biogeochemical turnover throughout Earth's history (e.g., Zheng et al., 2018; Grasby et al., 2019; Shen et al., 2019; Zerkle et al., 2020; Wu et al., 2022). In the pre-Anthropocene era, volcanism was the primary source of Hg in Earth's surface environment (Grasby et al., 2019). Volcanic Hg emitted to the atmosphere, mainly in gaseous Hg(0) form, has a sufficiently long residence time of 0.5–2 yr, allowing for its global transport and dispersion prior to deposition into terrestrial and ocean systems via wet and dry deposition pathways. Eventually, all Hg cycled through the environment enters the ocean via atmospheric deposition and terrestrial riverine runoff (Grasby et al., 2020), and is transferred into marine sediments by adsorption to organic matter and sulfide particles (Grasby et al., 2019). The seven natural Hg isotopes (196, 198-202, 204, amu) can undergo mass-dependent fractionation (Hg-MDF, reported as δ^{202}Hg) and mass-independent fractionation (Hg-MIF, denoted as Δ^{199}Hg, Δ^{200}Hg and Δ^{201}Hg). Hg-MDF results from various physical, chemical, and biological processes, whereas Hg-MIF is produced by photochemical processes in water bodies and cloud droplets (Bergquist and Blum, 2007; Blum et al., 2014). Hg undergoes redox transformations and photochemical reactions in the water column, and high levels of reduced sulfur in the photic zone may promote photo-reduction of S-bound Hg(II), resulting in negative Hg-MIF in the residual Hg(II) that is then recorded in marine sediments (Zheng et al., 2018). Post-depositional influence on sedimentary Hg isotopic signals is generally thought to be minor owing to the strong complexation of Hg and organic matter and reduced sulfur in sediments (Blum et al., 2014; Zheng et al., 2018; Zerkle et al., 2020; Chen et al., 2022). Hg concentrations and isotopes in ancient marine sediments thus have the potential to provide constraints on sources and cycling of Hg over geological times (Grasby et al., 2019).

2.2. Geological setting

The North China Craton is one of the main cratons underlying China (Fig. 1A). The Yanliao Basin of the North China Craton was an intracratonic rift basin formed with the breakup of the Columbia supercontinent (Chen et al., 2020). The sedimentary sequence of the Yanliao Basin was deposited in shallow subtidal to intertidal environments of the epicontinental sea (Fig. 1B; after Shi et al., 2021). The Proterozoic succession of the North China Craton is commonly divided into three groups, in ascending order (Fig. 1C): the Changcheng Group (1.8–1.6 Ga), the Jixian Group (1.6–1.4 Ga), and the Qingbaikou Group (1.0–0.8 Ga). A hiatus of ca. 400 Ma exists between the Jixian and Qingbaikou groups. We examined a drillcore JQ1 (40°35′05″N and 118°21′22″E) with sediments deposited in shallow water environments of the Yanliao Basin during the Mesoproterozoic (Fig. 1B). Our studied interval covers, in ascending order, the upper part of the Wumishan Formation, the Hongshuizhuang Formation, and the lower part of the Tieling Formation (Fig. 1D). The Wumishan Formation is mainly composed of dolomite and stromatolites formed under a peritidal environment. The Hongshuizhuang Formation was formed in a deeper subtidal to shallow water environment and consists of organic-rich black shale and muddy dolomite. The overlying Tieling Formation is dominated by dolomite formed in fluctuating peritidal to subtidal environments (Fig. 1D). U-Pb ages of 1483 ± 13 Ma for bentonite beds in the upper part of the Wumishan Formation (Li et al., 2014), and

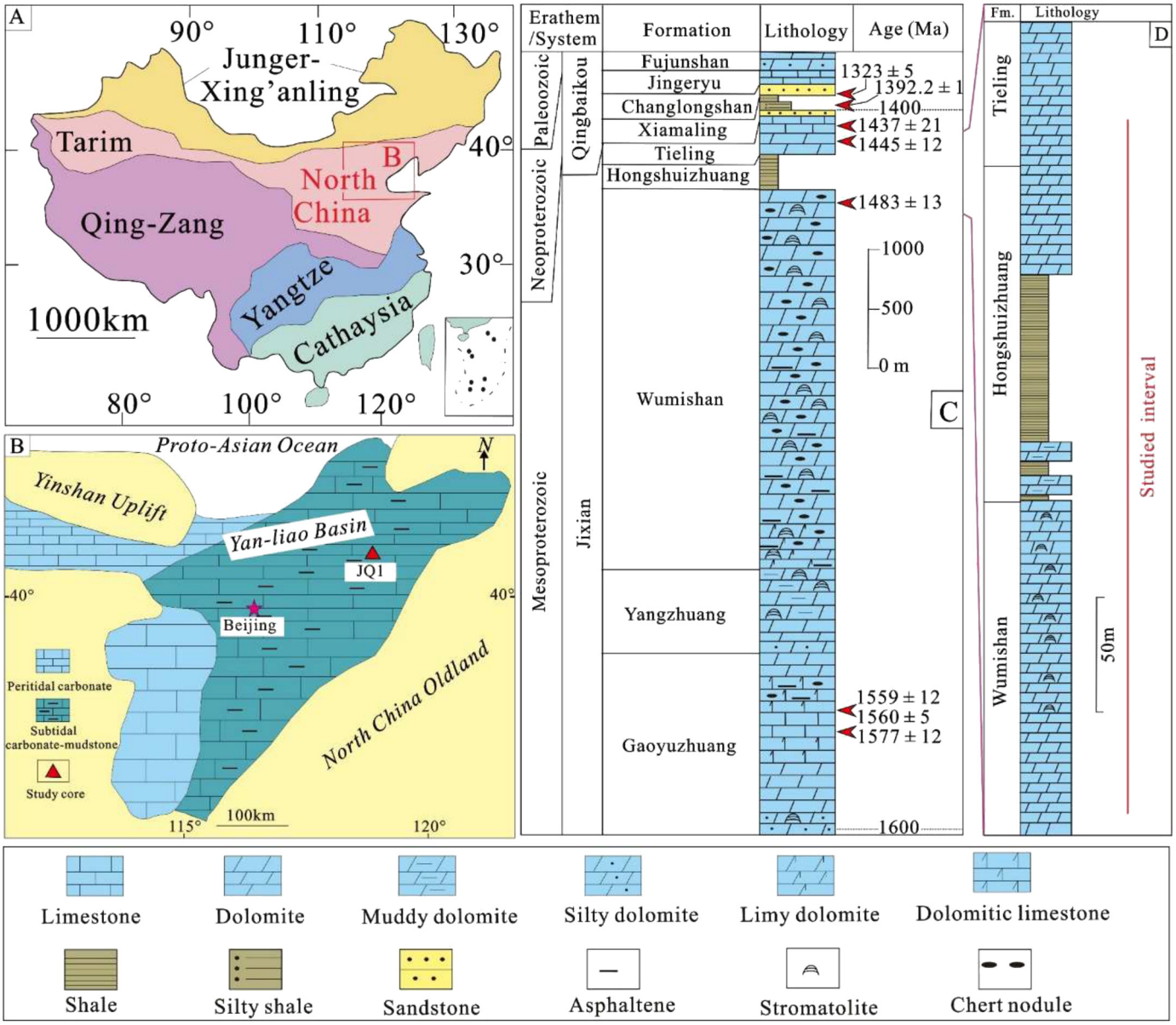

Fig. 1. Integrated diagrams showing geological setting of our study area. (A) Major tectonic units of China and the location of the North China Craton. The red box refers to the studied area in panel B. (B) Simplified paleogeographic map of Yanliao basin, North China Craton during the Mesoproterozoic Era (modified after Shi et al., 2021), and the location of our drillcore JQ1. (C) Stratigraphic subdivisions of Meso- to Neo-proterozoic Era in North China (modified after Luo et al., 2021) and stratigraphic ages summarized by Luo et al. (2021). (D) Stratigraphic columns of Wumishan, Hongshuizhuang, and Tieling Formations in our study area.

1437 ± 21 Ma for a K-bentonite bed in the lower part of the Tieling Formation (Su et al., 2010), define an age of ca. 1.5–1.4 Ga for our studied interval.

3. Samples and methods

3.1. Samples

Ninety nine (99) pieces of JQ1 core samples covering the Wumishan to Tieling formations were collected for total organic carbon (TOC) and total sulfur (TS) analyses. Among them, 85 samples were selected for total Hg concentrations analyses. Based on TOC, TS, and total Hg concentrations, 33 samples were further chosen for Hg isotope analyses. Samples were first cut into fresh chips, and then manually grounded to 200 mesh size using an agate mortar and pestle to avoid any metal contaminant. The powdered samples were dried and then preserved in a desiccator prior to chemical analysis.

3.2. TOC and TS concentrations

The powdered samples (80–120 mg) were treated with 2 M HCl until carbonates have been removed thoroughly, and then washed using deionized water, and dried at 60 °C overnight before instrumental analysis. TOC and TS contents were measured respectively on HCl-treated and non-treated samples using a Leco CS230 carbon/sulfur analyzer at the Guangzhou Institute of Geochemistry, Chinese Academy of Sciences (CAS). The precision of TOC and TS measurements is generally better than 0.3% based on standard and duplicate samples.

3.3. Total Hg concentrations

Total Hg concentrations were determined using a Lumex R915A direct combustion system at the Institute of Geochemistry, CAS. The measurement precision of Hg concentration was monitored by procedural blanks, standard reference materials (GSS-5, soil, n=14,

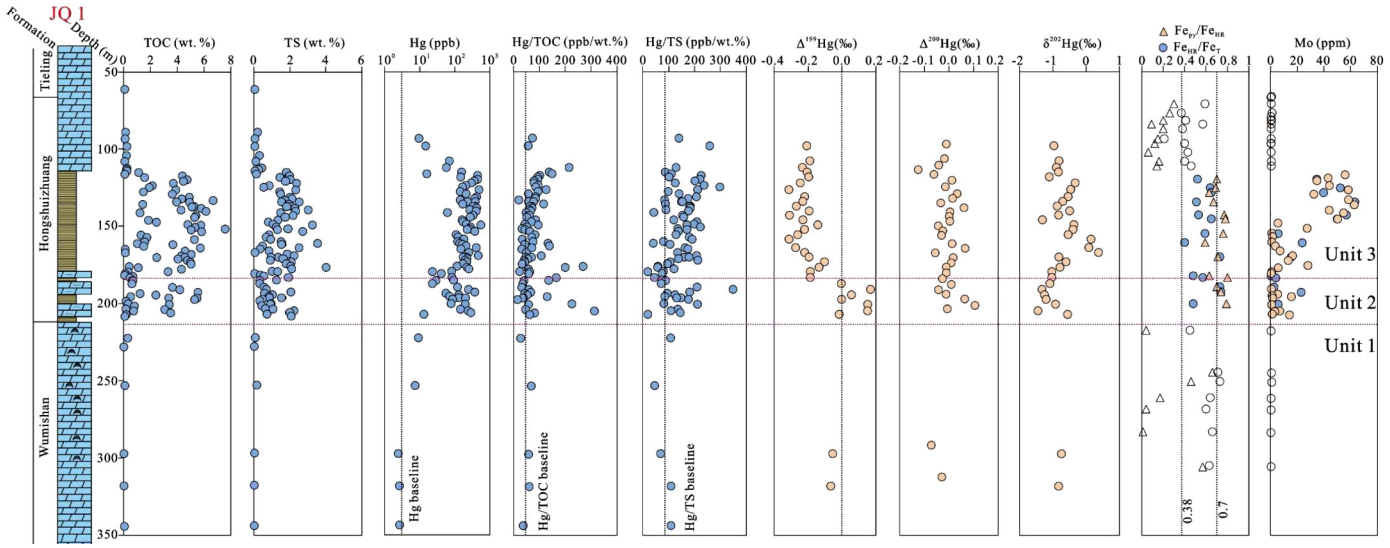

Fig. 2. Stratigraphic profiles of TOC, TS and Hg concentrations, Hg/TOC and Hg/TS ratios, Hg isotopes, Fe speciation data and Mo concentrations for JQ1 core samples. Fe speciation data of JQ1 core samples are from Chen et al. (2020). Mo concentrations of JQ1 core samples marked by blue circles are from Chen et al. (2020), and those marked by orange circles are adopted from Luo et al. (2013). It is worthy to note that Fe speciation data (open circles and triangles) and Mo concentrations (open circles) of dolomite samples are intentionally marked to take caution for their redox interpretation.

290 ppb) and sample duplicates. The Hg concentration of procedural blanks is generally less than 1% of Hg concentration in samples. Generally, measurements of standard reference material (GSS-5) showed recoveries of 90–110%, and measurement errors for triplicate analyses were < 7%.

3.4. Hg isotopes analysis

Two validated methods were used for Hg pre-concentration. For low Hg samples (< 25 ppb), a double-stage tube furnace coupled with 10 mL of 40% mixed acid solutions (HNO_3/HCl = 2/1, v/v) were used for pre-concentration following the procedure described by Zerkle et al. (2020). For samples with high Hg concentrations (>25 ppb), an acid digestion method using mixed acid solutions (HNO_3/HCl = 1/3, v/v) was used to prepare the samples (Yin et al., 2016). GSS-4 soil standard reference materials were prepared using both methods. All the solutions yielded from the two pretreatment methods were diluted to 0.5 ng/mL Hg, with an acidity of ~10%, and then used for Hg isotope measurement using a Neptune Plus multi-collector inductively coupled plasma mass spectrometry at the Institute of Geochemistry, CAS, following the procedure described by Yin et al. (2016). NIST SRM 3133 Hg standard solutions with matrix and concentration similar to sample dilutions were used for mass bias using standard-sample bracketing. Total Hg concentrations in samples were monitored by MC-ICP-MS using ^{202}Hg signals (~1.70 V per ng/mL). The Hg recoveries of the samples were 87–109% of those measured with the Lumex R915A Hg analyzer. The Hg recoveries of GSS-4 were 90–110% of the recommended values (~290 ng/g). As recommended by Blum and Bergquist (2007), Hg isotopes are reported as delta values (δ) in per mil (‰) relative to the analyzed NIST SRM 3133, following the Equation (1):

$$\delta^{XXX}\mathrm{Hg}(‰) = \left[\frac{\left(\frac{XXX_{Hg}}{198_{Hg}}\right)_{sample}}{\left(\frac{XXX_{Hg}}{198_{Hg}}\right)_{NIST\ SRM3133}} - 1\right] \times 1000 \quad (1)$$

Mass-independent fractionation (MIF) is reported in Δ notation (Δ^{XXX} Hg), which describes the difference between the measured δ^{XXX}Hg and theoretically predicted δ^{XXX}Hg values, using Equation (2):

$$\Delta^{XXX}\mathrm{Hg}\,(‰) = \delta^{XXX}\mathrm{Hg}_{sample} - \beta \times \delta^{202}\mathrm{Hg}_{sample} \quad (2)$$

where β values are 0.2520 for ^{199} Hg, 0.5024 for ^{200} Hg, and 0.7520 for ^{201} Hg, respectively. The overall average and uncertainty of NIST-3177 (δ^{202}Hg: −0.53 ± 0.05‰; Δ^{199}Hg: −0.01 ± 0.04‰; Δ^{200}Hg: 0.00 ± 0.06‰, 2SD, n = 10) and GSS-4 (δ^{202}Hg: −1.66 ± 0.10‰; Δ^{199}Hg: −0.35 ± 0.09‰; Δ^{200}Hg: 0.00 ± 0.08‰, 2SD, n = 6) (*Supplementary Table S3*) agree well with previously published results (Bergquist and Blum, 2007). Analytical uncertainty of our samples was estimated based on the larger 2SD values of that for NIST-3177 or GSS-4.

4. Results

Measured Hg, TOC and TS concentrations, Hg/TOC and Hg/TS ratios as well as Hg isotopic compositions of JQ1 core samples are listed in *Supplementary Tables S1 and S2* and presented in Fig. 2. Early published results of redox proxies (Fe speciation and Mo concentrations) for JQ1 core samples (Luo et al., 2013; Chen et al., 2020) are also compiled in Fig. 2. Based on dramatic changes in Hg isotope and published redox proxies (Fe speciation and Mo concentrations), three units are defined to carefully investigate the major changes in oceanic chemistry (Fig. 2). Unit 1 (207.2–344.3 m) shows extremely low TOC (0.03–0.3 wt%), TS (0.02–0.17 wt%), and Hg concentrations (2.4–9.1 ppb) as well as relatively low ratios of Hg/TOC (28–69 ppb/wt%) and Hg/TS (44–110 ppb/wt%). Near-zero Δ^{199}Hg values (−0.07 to −0.05‰) and negative δ^{202}Hg values (−0.83 to −0.74‰) are observed in two samples of this unit. Unit 2 (185.1–207.2 m) shows relatively high levels of TOC (0.20–5.56 wt%), TS (0.33–2.22 wt%), and Hg concentrations (16.1–312.6 ppb). Hg/TOC ratios of Unit 2 generally vary around low values of 16.1–81.6 ppb/wt%, except several peaks (up to 312.6 ppb/wt%), while Hg/TS ratios of Unit 2 are variable, fluctuating between 17.6 and 350.9 ppb/wt%. Near-zero to positive Δ^{199}Hg values (−0.02 to +0.17‰) as well as negative δ^{202}Hg values (−1.33 to −0.56‰) are observed in Unit 2. Unit 3 (61.1–185.1 m) shows relatively high TOC (0.10–6.59 wt%), TS (0.04–4.03 wt%) and Hg concentrations (9.4–554.8 ppb) as well as relatively stable Hg/TOC ratios (21–102 ppb/wt%) except few peaks (up to 269 ppb/wt%) and relatively high

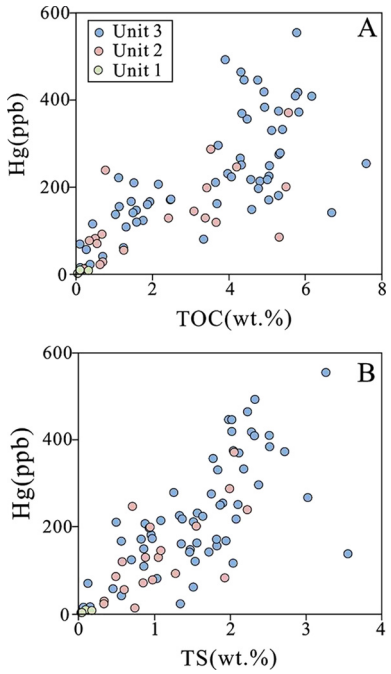

Fig. 3. Cross plots of Hg vs TOC (A) and Hg vs TS (B) for JQ1 core samples.

Hg/TS ratios (17–299 ppb/wt%). Notably, most negative Δ^{199}Hg values (−0.31 to −0.10‰) and variable δ^{202}Hg values (−1.31 to +0.37‰) appear in Unit 3 (Fig. 2).

5. Discussion

5.1. Background terrestrial Hg deposition (Unit 1)

Hg enrichment in marine sediments is commonly caused by either excessive Hg inputs (e.g., volcanism, hydrothermal venting, and terrestrial soil erosion) or particular redox conditions (e.g., anoxic and euxinic) (Zheng et al., 2018; Grasby et al., 2019; Shen et al., 2019). Such processes may also result in abnormally high Hg/TOC or Hg/TS ratios in sediments, because aqueous Hg in seawater is mainly transferred into marine sediments by adsorption onto organic matter and sulfur particles (Grasby et al., 2019). In contrast, the relatively low Hg concentration along with low ratios of Hg/TOC and Hg/TS in sediments may suggest background seawater Hg deposition without external sources and redox change (Fan et al., 2021). The positive correlations of Hg and TOC or Hg and TS (Fig. 3A and 3B) indicate Hg is removed from seawater either via organic matter or sulfide particles in our samples. Although high Fe_{HR}/Fe_T ratios of Unit 1 samples (> 0.38) indicate anoxic bottom water condition, they may be magnified by the extremely low Fe_T (< 0.5%) of Wumishan carbonates and thus cannot provide reliable redox information (Chen et al., 2020). Alternatively, according to sedimentological sequence, the shallow water carbonate as well as abundant stromatolites suggests that Unit 1 was deposited under a stable oxic environment (Chen et al., 2020). The extremely low Hg, TOC and TS concentrations as well as low Hg/TOC and Hg/TS ratios for Unit 1 samples may thus act as a baseline of background Hg deposition in this study (Fig. 2).

Both Hg-MIF and Hg-MDF could provide constraints on Hg sources (Yin et al., 2016). The Δ^{199}Hg values in marine sediments are generally balanced by two end members, i.e., atmospheric Hg carrying positive Δ^{199}Hg and terrestrial Hg carrying negative to near-zero Δ^{199}Hg (Grasby et al., 2019). The near-zero Δ^{199}Hg values of Unit 1 are between modern seawater end-member (mean values of +0.16 ± 0.10‰; Štrok et al., 2015) and modern terrestrial soils end-member (mean values of −0.25 ± 0.14‰; Sun et al., 2019) (Fig. 4A). However, δ^{202}Hg values of Unit 1 (−0.83 to −0.74‰) are less negative than those values of either terrestrial soils (−1.79 ± 0.45‰; Sun et al., 2019) or modern seawater (−1.73 ± 0.72‰; Štrok et al., 2015) end-members (Fig. 4A). It is worthy to note that due to the lack of terrestrial plant vegetation and soils in the Precambrian period, Hg isotopes of the terrestrial end member are most likely more similar to those of volcanic ash and silicate rocks, i.e., Δ^{199}Hg of ~ 0‰ and less negative δ^{202}Hg of ~ −0.6‰ to −0.1‰ (Fan et al., 2021; Meixnerova et al., 2021; Wu et al., 2022). Recently, a case study of near-shore Mesoproterozoic sediments (1.57 Ga) in the same Yanliao basin also displays a terrestrial Δ^{199}Hg end member of close to 0‰ (Tang et al., 2022). Both near-zero Δ^{199}Hg and less negative δ^{202}Hg values of Unit 1 are consistent with those of a Precambrian terrestrial end member, most likely reflecting background terrestrial Hg isotopic signals due to its nearshore environment (Fig. 5A).

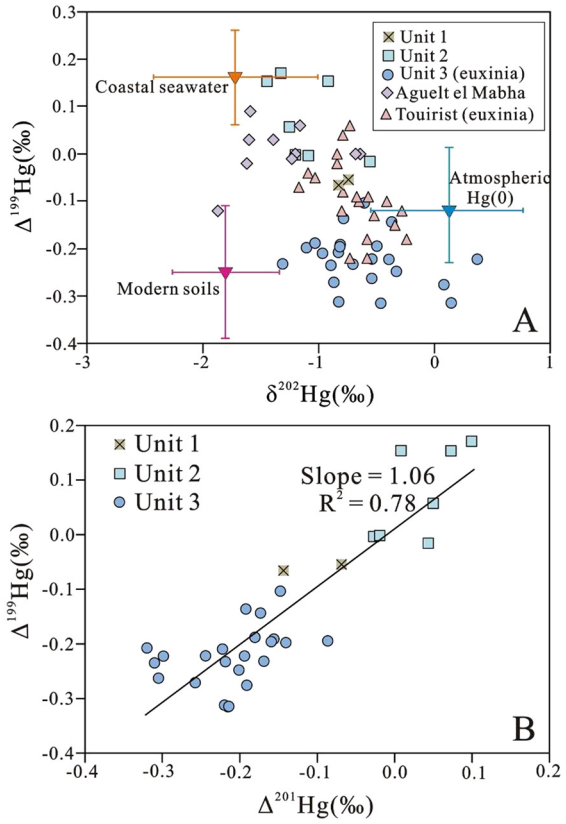

Fig. 4. Cross plots of Δ^{199}Hg vs δ^{202}Hg (A) and Δ^{199}Hg vs Δ^{201}Hg (B) for JQ1 core samples (this study) and Aguelt el Mabha and Touirist Formation (1.1 Ga) sediments (Zheng et al., 2018). The mean Δ^{199}Hg and δ^{202}Hg values of modern coastal seawater are sourced from Štrok et al. (2015). The mean Δ^{199}Hg and δ^{202}Hg values of modern soils (n= 85) and atmospheric Hg(0) (n= 220) are based on compiled data by Sun et al. (2019).

5.2. Atmospheric Hg(II) deposition into oxic surface waters (Unit 2)

The Unit 2 samples are characterized with $Fe_{HR}/Fe_T > 0.38$ and $Fe_{py}/Fe_{HR} > 0.7$, suggesting euxinic bottom water conditions (Fig. 2; Chen et al., 2020). Such H_2S-rich bottom waters promote more efficient Hg burial associated with enhanced drawdown of organic matter and sulfide particles, resulting in high levels of Hg concentration as observed in Unit 2 samples. Several peaks of Hg/TOC and high levels of Hg/TS ratios are higher than those of our defined Hg baseline in Unit 1, suggesting that Hg enrichment is not solely caused by enhanced organic matter and sulfide burial, but is also linked to an increased Hg flux to the ocean. The near-zero Δ^{199}Hg values in some samples of Unit 2 are comparable

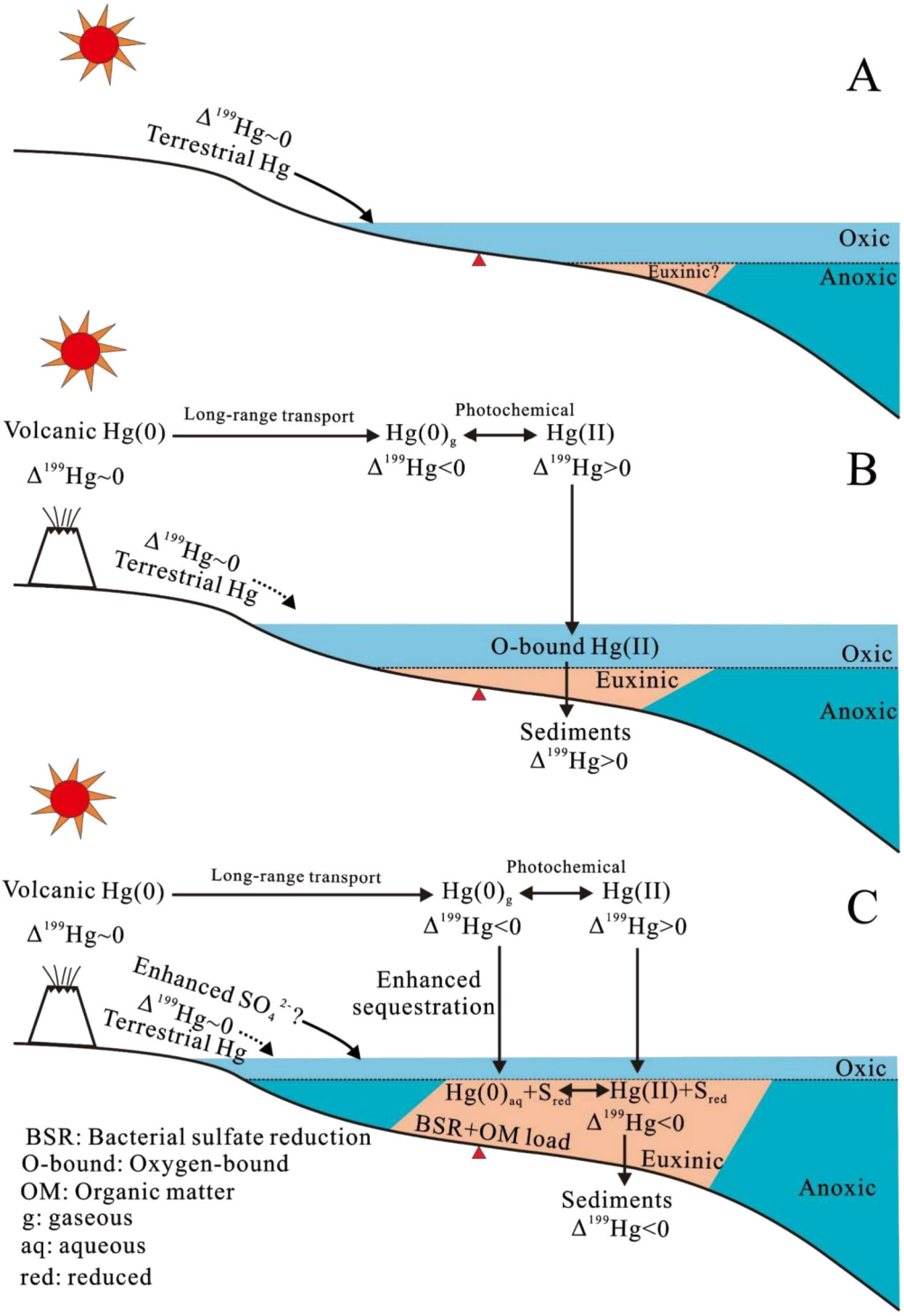

Fig. 5. Simplified diagram showing Hg cycle and redox variation in the Meso-proterozoic ocean. (A) background terrestrial Hg into the stratified ocean (Unit 1). (B) The deposition of atmospheric Hg(II) into oxic surface waters and the transfer of O-bound Hg(II) to sediments (Unit 2). (C) Enhanced sequestration of gaseous Hg(0) and photo-reduction of reduced sulfur-bound Hg(II) in response to the euxinia of the photic zone (Unit 3).

to the background terrestrial Δ^{199}Hg signals of Unit 1. However, some samples show positive Δ^{199}Hg values similar to those of modern seawater and open-ocean marine sediments (Štrok et al., 2015; Grasby et al., 2019), which may indicate a dramatic change in Hg sources. During the Precambrian, volcanic Hg(0), carrying near-zero Δ^{199}Hg, was the primary source of Hg to environment (Zerkle et al., 2020). The emitted Hg(0) underwent photochemical processes during long-distance transport, triggering negative Δ^{199}Hg in the gaseous Hg(0) pool and positive Δ^{199}Hg in the atmospheric Hg(II) pool (Bergquist and Blum, 2007). Seawater generally receives water-soluble atmospheric Hg(II) carrying a positive Δ^{199}Hg signal, which is then transferred from seawater to sediments, and thus resulting in positive Δ^{199}Hg values as usually observed in marine sediments over geological time (Grasby et al., 2019). Moreover, in an oxic water column, photo-reduction of Hg(II) bound to oxygen-containing ligands triggers positive Δ^{199}Hg in the residual Hg(II) that is also inherited by sediments (Zheng et al., 2018). Although the relationship between Δ^{199}Hg and Δ^{200}Hg

is not significant (Fig. 2), the most positive Δ^{200}Hg of Unit 2 is coupled with positive Δ^{199}Hg, which can be another evidence of enhanced deposition of atmospheric oxidized Hg(II) (Gratz et al., 2010). Therefore, positive Δ^{199}Hg in some samples of Unit 2 may suggest atmospheric Hg(II) deposition into oxic surface waters after long-distance transportation from volcano sites (Fig. 5B). Although the Fe speciation data suggest euxinic bottom waters (Chen et al., 2020), our Hg results reveal that surface waters remained oxic and were overlying euxinic bottom waters, which is consistent with the general model for redox-stratified Mesoproterozoic oceans (Poulton and Canfield, 2011).

5.3. Enhanced sequestration of Hg(0) and photo-reduction of reduced sulfur-bound Hg(II) as a result of photic zone euxinia (Unit 3)

The $Fe_{HR}/Fe_T > 0.38$ and $Fe_{py}/Fe_{HR} > 0.7$ of Unit 3 samples indicate euxinic bottom water conditions (Fig. 2; Chen et al., 2020). Furthermore, Mo concentrations in sediments become strongly enriched under euxinic water conditions owing to efficient burial of Mo in the form of thiomolybdates (e.g., Anbar and Knoll, 2002). Thus, the high level of Mo concentrations (up to 60 ppm) in Unit 3 samples may also support strong H_2S-rich bottom water conditions (Fig. 2; Luo et al., 2013; Chen et al., 2020). The observation of Hg enrichment for Unit 3 samples may be ascribed to rapid scavenging of seawater Hg by sulfide and organic matter particulates under euxinic bottom water conditions. The negative Δ^{199}Hg values (as low as −0.3‰) are lower than background terrestrial Hg signals (Δ^{199}Hg ∼ 0‰) of Unit 1 and atmospheric Hg(II) deposition (Δ^{199}Hg > 0‰) of Unit 2. Such abnormally negative Δ^{199}Hg values are also lower than those of Phanerozoic marine sediments (−0.1 to +0.4‰), but are comparable to those of Archean and Proterozoic marine sediments (Fig. 6), perhaps linked to unique atmospheric and oceanic chemistry of early Earth. Four scenarios may be responsible for the negative shifting of Δ^{199}Hg in Unit 3: 1) abiotic non-photochemical reduction of Hg(II) by oceanic dissolved organic matter (Zheng and Hintelmann, 2010a); 2) the deposition of gaseous Hg(0) absorbed on organic aerosols into ocean and sediments (Zerkle et al., 2020); 3) enhanced sequestration of atmospheric Hg(0) to the sediments by thiols and sulfides that were enriched in the H_2S-rich photic zone (Zheng et al., 2013, 2018); and 4) photo-reduction of seawater Hg(II) bound with reduced sulfur as a result of photic zone euxinia (Zheng and Hintelmann, 2010b; Zheng et al., 2018).

According to experimental observation, non-photochemical reduction of Hg(II) triggers negative Δ^{199}Hg in residual Hg(II) (Zheng and Hintelmann, 2010a). However, the slope of the linear regression between Δ^{199}Hg and Δ^{201}Hg in the case of non-photochemical process is around 1.6 (Zheng and Hintelmann, 2010a), which is much different from the Δ^{199}Hg/Δ^{201}Hg slope of 1.06 for our samples (Fig. 4B). The background atmospheric Hg(0) generally displays a mean Δ^{199}Hg value of −0.11 ± 0.12‰ (Sun et al., 2019), and the similarly negative Δ^{199}Hg values observed in Unit 3 samples may reflect a net source of atmospheric Hg(0) to the ocean and sediments. Given that only Hg(II) species are reactive and water-soluble, the transfer of atmospheric gaseous Hg(0) signals into sediments require that they are oxidized to Hg(II) species in the atmosphere or surface ocean (Zheng et al., 2018; Zerkle et al., 2020). The hydrocarbon-rich haze with high atmospheric CH_4:CO_2 ratios may induce oxidation and sequestration of gaseous Hg(0) and transport these negative Hg-MIF signals to ocean and sediments, like those observed in the late Archean Era (Zerkle et al., 2020). However, the formation of organic aerosol hazes was evidenced by S-MIF and $\delta^{13}C_{org}$ values of late Archean sediments (Zerkle et al., 2020), but there is no available evidence supporting their occurrence in the Mesoproterozoic atmosphere, making scenario 2 less likely. Based on experimental observations,

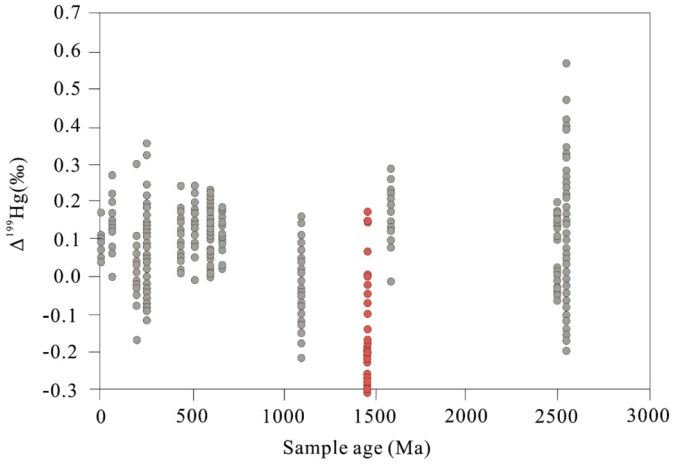

Fig. 6. Compiled Δ^{199}Hg data of marine sediments over geological time. The red circles represent the range of Δ^{199}Hg in this study. The Δ^{199}Hg values of Phanerozoic sediments are compiled by Zerkle et al. (2020). The Δ^{199}Hg values of Mesoproterozoic sediments (ca. 1.1 Ga and 1.57 Ga) are from Zheng et al. (2018) and Tang et al. (2022), respectively. The published Δ^{199}Hg values of Archean sediments are from Blum et al. (2014) and Zerkle et al. (2020), respectively.

the presence of thiols in a sulfide-rich photic zone may accelerate the oxidation of atmosphere-sourced Hg(0) to Hg(II) and subsequent sequestration to marine sediments (Zheng et al., 2013). In addition, photo-reduction of Hg(II) complexed by reduced sulfur ligands in the photic zone also shifts additionally negative Hg-MIF signals to sediments (Zheng and Hintelmann, 2010b; Zheng et al., 2018). These two mechanisms (scenarios 3 and 4) have been invoked to explain the negative Δ^{199}Hg value of around −0.2‰ in Mesoproterozoic (∼1.1 Ga) Touirist euxinic shales (Zheng et al., 2018). Notably, Δ^{199}Hg values of some samples in Unit 3 (as low as −0.31‰) are even more negative than those of modern atmospheric Hg (0) and 1.1 Ga Touirist shale (Fig. 4A). So, enhanced sequestration of atmospheric Hg (0) alone (scenario 3) is not enough to produce such abnormally negative Δ^{199}Hg values, and the photo-reduction of Hg(II) by reduced sulfur (scenario 4) may be required. Note that both scenarios 3 and 4 require a sulfide-rich photic zone to sustain high concentrations of reduced thiols and sulfide. In addition, the negative shift of Δ^{199}Hg in Unit 3 samples is coupled with positive δ^{202}Hg (Fig. 4A), which is also consistent with those observed in Touirist euxinic shales (Zheng et al., 2018), perhaps linked to enhanced sequestration of atmospheric Hg(0) carrying positive δ^{202}Hg signals in an euxinic photic zone. As discussed above, although there are still some uncertainties, photic zone euxinia seems to be the most plausible explanation for our negative Δ^{199}Hg values, especially in the context of Mesoproterozoic atmospheric and oceanic systems, at least within the scope of current knowledge. Therefore, we consider that the negative shift of Δ^{199}Hg may be caused by the expansion of euxinic waters from the mid-depth to the photic zone (Fig. 5C).

5.4. Possible cause of dynamic euxinia and implications for eukaryotic evolution in the Mesoproterozoic Era

It is worth to note that the abnormally negative Δ^{199}Hg values of 1.5−1.4 Ga (this study) and 1.1 Ga (Zheng et al., 2018) euxinic organic-rich shales (Fig. 6) correspond to the same periods of transient increase in oxygen levels based on I/(Ca+Mg) ratios and Cr isotope (Hardisty et al., 2017; Canfield et al., 2018). The oxidative weathering input of SO_4^{2-} into shallow water environment may be episodically enhanced during the rise of O_2 level, forming H_2S-rich water column through bacterial sulfate reduction (BSR) process. When enhanced SO_4^{2-} input is coincidentally superimposed with high organic matter (OM) flux in some areas (but not in the whole

basin), such as the Unit 3 with TOC contents up to 7.6%, the rate of BSR will be accelerated, likely leading to episodic expansion of euxinia to the photic zone as recorded by negative Δ^{199}Hg (Fig. 5C). Therefore, the dynamic euxinia may be closely related to the cooperation of oxidative weathering input of SO_4^{2-} and OM flux in the water column.

Although the oxygen requirements of Mesoproterozoic eukaryotes were considered to be lower than generally thought, oxygenation still acts as an important key factor for the evolution of complex eukaryotes (e.g., Zhang et al., 2016, 2018). Given eukaryotic fossils were commonly restricted to shallow environments in the Mesoproterozoic Era (Javaux et al., 2001), redox structure of shallow settings may have a significant influence on the evolution of eukaryotes (Gilleaudeau and Kah, 2015; Doyle et al., 2018). The extent of euxinia in a shallow environment would have a specific role in the diversification of eukaryote owing to the rapid sequestration of bio-essential elements (e.g., Mo, Zn) in H_2S-rich waters (Anbar and Knoll, 2002). Our highly fractionated Hg isotope data reveal the expansion of dynamic euxinia to the photic zone, thus severely limiting the habitat of eukaryotes. Widespread euxinia of the surface ocean has also been considered as a killing mechanism for major Phanerozoic mass extinction events (Whiteside and Grice, 2016). Thus, we propose that the dynamic euxinia of shallow waters may have been an episodic limiting factor for diversification of early life in the Mesoproterozoic oceans.

6. Conclusions

Our new Hg-C-S geochemistry data, associated with published redox proxies, from ca. 1.5–1.4 Ga sediments of the Yanliao Basin reveal a new redox structure of dynamic euxinia in shallow waters of the Mesoproterozoic ocean. High levels of Hg concentrations in Units 2 and 3 samples are ascribed to more efficient Hg burial along with enhanced drawdown of organic matter and sulfide particles. The near-zero Δ^{199}Hg values of unit 1 most likely reflect background terrestrial Hg signals, and positive Δ^{199}Hg values of unit 2 suggest atmospheric Hg(II) deposition into oxic surface waters. Whereas, the abnormally negative Δ^{199}Hg values of unit 3 may be caused by enhanced sequestration of gaseous Hg(0) and photo-reduction of reduced sulfur-bound Hg(II) in response to photic zone euxinia. Our highly fractionated Hg isotope data reveal that the extent of euxinia was dynamic, and that it may have expanded to the photic zone, which may have played a significant role in the evolution of eukaryote of the Mesoproterozoic oceans.

CRediT authorship contribution statement

All authors have contributed to this work. **H. Tian:** Resources, Conceptualization, Supervision, Writing - Revised version and Funding acquisition; **Y.W. Wu:** Investigation, Visualization and Writing - Original Draft; **R.S. Yin:** Resources, Data Curation and Formal analysis; **D. Chen:** Data Curation; **S.E. Grasby:** Formal analysis; **J. Shen:** Formal analysis; **T.F. Li:** Data Curation; **S. Ji:** Visualization; **P.A. Peng:** Formal analysis and Writing - Revised version.

Declaration of competing interest

The authors declare that they have no known competing financial interests or personal relationships that could have appeared to influence the work reported in this paper.

Data availability

Data will be made available on request.

Acknowledgements

This study was supported by the Natural Science Foundation of China (41925014). The Editor Boswell Wing and two anonymous reviewers are thanked for their constructive comments and suggestions that greatly improved the whole quality of the manuscript. This is contribution No. IS-3351 from GIGCAS.

Appendix A. Supplementary material

Supplementary material related to this article can be found online at https://doi.org/10.1016/j.epsl.2023.118211.

References

Anbar, A.D., Knoll, A.H., 2002. Proterozoic ocean chemistry and evolution: a bioinorganic bridge? Science 297, 1137–1142.
Anbar, A.D., Duan, Y., Lyons, T.W., Arnold, G.L., Kendall, B., Creaser, R.A., Kaufman, A.J., Gordon, G.W., Scott, C., Garvin, J., Buick, R., 2007. A whiff of oxygen before the great oxidation event? Science 317, 1903–1906.
Bergquist, B.A., Blum, J.D., 2007. Mass-dependent and -independent fractionation of Hg isotopes by photoreduction in aquatic systems. Science 318, 417–420.
Blum, J.D., Bergquist, B.A., 2007. Reporting of variations in the natural isotopic composition of mercury. Anal. Bioanal. Chem. 388, 353–359.
Blum, J.D., Sherman, L.S., Johnson, M.W., 2014. Mercury isotopes in Earth and environmental sciences. Annu. Rev. Earth Planet. Sci. 42, 249–269.
Brocks, J.J., Love, G.D., Summons, R.E., Knoll, A.H., Logan, G.A., Bowden, S.A., 2005. Biomarker evidence for green and purple sulphur bacteria in a stratified Palaeoproterozoic sea. Nature 437, 866–870.
Brocks, J.J., 2011. Millimeter-scale concentration gradients of hydrocarbons in Archean shales: live-oil escape or fingerprint of contamination? Geochim. Cosmochim. Acta 75, 3196–3213.
Canfield, D.E., 1998. A new model for Proterozoic ocean chemistry. Nature 396, 450–453.
Canfield, D.E., Zhang, S., Frank, A.B., Wang, X., Wang, H., Su, J., Ye, Y., Frei, R., 2018. Highly fractionated chromium isotopes in Mesoproterozoic-aged shales and atmospheric oxygen. Nat. Commun. 9, 2871.
Chen, X.Y., Li, M.H., Sperling, E.A., Zhang, T.G., Zong, K.Q., Liu, Y.S., Shen, Y.N., 2020. Mesoproterozoic paleo-redox changes during 1500-1400 Ma in the Yanshan Basin, North China. Precambrian Res. 347, 105835.
Chen, D., Ren, D., Deng, C., Tian, Z., Yin, R., 2022. Mercury loss and isotope fractionation during high-pressure and high-temperature processing of sediments: implication for the behaviors of mercury during metamorphism. Geochim. Cosmochim. Acta 334, 231–240.
Doyle, K.A., Poulton, S.W., Newton, R.J., Podkovyrov, V.N., Bekker, A., 2018. Shallow water anoxia in the Mesoproterozoic ocean: evidence from the Bashkir Meganticlinorium, Southern Urals. Precambrian Res. 317, 196–210.
Eickmann, B., Hofmann, A., Wille, M., Bui, T.H., Wing, B.A., Schoenberg, R., 2018. Isotopic evidence for oxygenated Mesoarchaean shallow oceans. Nat. Geosci. 11, 133–138.
Fan, H.F., Fu, X.W., Ward, J.F., Yin, R.S., Wen, H.J., Feng, X.B., 2021. Mercury isotopes track the cause of carbon perturbations in the Ediacaran ocean. Geology 49, 248–252.
Gilleaudeau, G.J., Kah, L.C., 2015. Heterogeneous redox conditions and a shallow chemocline in the Mesoproterozoic ocean: evidence from carbon-sulfur-iron relationships. Precambrian Res. 257, 94–108.
Gratz, L.E., Keeler, G.J., Blum, J.D., Sherman, L.S., 2010. Isotopic composition and fractionation of mercury in Great Lakes precipitation and ambient air. Environ. Sci. Technol. 44, 7764–7770.
Grasby, S.E., Them II, T.R., Chen, Z., Yin, R., Ardakani, O.H., 2019. Mercury as a proxy for volcanic emissions in the geologic record. Earth-Sci. Rev. 196, 102880.
Grasby, S.E., Liu, X.J., Yin, R.S., Ernst, R.E., Chen, Z.H., 2020. Toxic mercury pulses into late Permian terrestrial and marine environments. Geology 48, 830–833.
Hardisty, D.S., Lu, Z.L., Bekker, A., Diamond, C.W., Gill, B.C., Jiang, G.Q., Kah, L.C., Knoll, A.H., Loyd, S.J., Osburn, M.R., Planavsky, N.J., Wang, C.J., Zhou, X.L., Lyons, T.W., 2017. Perspectives on Proterozoic surface ocean redox from iodine contents in ancient and recent carbonate. Earth Planet. Sci. Lett. 463, 159–170.
Javaux, E.J., Knoll, A.H., Walter, M.R., 2001. Morphological and ecological complexity in early eukaryotic ecosystems. Nature 412, 66–69.
Knoll, A.H., Carroll, S.B., 1999. Early animal evolution: emerging views from comparative biology and geology. Science 284, 2129–2137.
Li, H., Su, W., Zhou, H., Xiang, Z., Tian, H., Yang, L., Huff, D.W., Ettensohn, R.F., 2014. The first precise age constraints on the Jixian System of the Meso- to Neoproterozoic Standard Section of China: SHRIMP zircon U-Pb dating of bentonites from the Wumishan and Tieling formations in the Jixian Section, North China Craton. Acta Petrol. Sin. 30, 2999–3012.

Luo, Q.Y., Zhong, N.N., Zhu, L., Wang, Y.N., Qin, J., Qi, L., Zhang, Y., Ma, Y., 2013. Correlation of burial organic carbon and paleoproductivity in the Mesoproterozoic Hongshuizhuang Formation, northern North China. Chin. Sci. Bull. 58, 1299–1309.

Luo, Q.Y., George, S.C., Xu, Y.H., Zhong, N.N., 2016. Organic geochemical characteristics of the Mesoproterozoic Hongshuizhuang Formation from northern China: implications for thermal maturity and biological sources. Org. Geochem. 99, 23–37.

Luo, G., Junium, C.K., Kump, L.R., Huang, J., Li, C., Feng, Q., Shi, X., Bai, X., Xie, S., 2014. Shallow stratification prevailed for ∼1700 to ∼1300 Ma ocean: evidence from organic carbon isotopes in the North China Craton. Earth Planet. Sci. Lett. 400, 219–232.

Luo, J., Long, X.P., Bowyer, F.T., Mills, B.J.W., Li, J., Xiong, Y.J., Zhu, X.K., Zhang, K., Poulton, S.W., 2021. Pulsed oxygenation events drove progressive oxygenation of the early Mesoproterozoic ocean. Earth Planet. Sci. Lett. 559, 116754.

Lyons, T.W., Reinhard, C.T., Planavsky, N.J., 2014. The rise of oxygen in Earth's early ocean and atmosphere. Nature 506, 307–315.

Meixnerova, J., Blum, J.D., Johnson, M.W., Stueken, E.E., Kipp, M.A., Anbar, A.D., Buick, R., 2021. Mercury abundance and isotopic composition indicate subaerial volcanism prior to the end-Archean "whiff" of oxygen. Proc. Natl. Acad. Sci. USA 118, e2107511118.

Planavsky, N.J., McGoldrick, P., Scott, C.T., Li, C., Reinhard, C.T., Kelly, A.E., Chu, X.L., Bekker, A., Love, G.D., Lyons, T.W., 2011. Widespread iron-rich conditions in the mid-Proterozoic ocean. Nature 477, 448–451.

Planavsky, N.J., Reinhard, C.T., Wang, X.L., Thomson, D., McGoldrick, P., Rainbird, R.H., Johnson, T., Fischer, W.W., Lyons, T.W., 2014. Low Mid-Proterozoic atmospheric oxygen levels and the delayed rise of animals. Science 346, 635–638.

Planavsky, N.J., Slack, J.F., Cannon, W.F., O'Connell, B., Isson, T.T., Asael, D., Jackson, J.C., Hardisty, D.S., Lyons, T.W., Bekker, A., 2018. Evidence for episodic oxygenation in a weakly redox-buffered deep mid-Proterozoic ocean. Chem. Geol. 483, 581–594.

Poulton, S.W., Fralick, P.W., Canfield, D.E., 2010. Spatial variability in oceanic redox structure 1.8 billion years ago. Nat. Geosci. 3, 486–490.

Poulton, S.W., Canfield, D.E., 2011. Ferruginous conditions: a dominant feature of the ocean through Earth's history. Elements 7, 107–112.

Shen, J., Chen, J.B., Algeo, T.J., Yuan, S.L., Feng, Q.L., Yu, J.X., Zhou, L., O'Connell, B., Planavsky, N.J., 2019. Evidence for a prolonged Permian-Triassic extinction interval from global marine mercury records. Nat. Commun. 10, 1563.

Shi, Q., Shi, X.Y., Tang, D.J., Fan, C.H., Wei, B.L., Li, Y., 2021. Heterogeneous oxygenation coupled with low phosphorus bio-availability delayed eukaryotic diversification in Mesoproterozoic oceans: evidence from the ca 1.46 Ga Hongshuizhuang Formation of North China. Precambrian Res. 354, 106050.

Sperling, E.A., Rooney, A.D., Hays, L., Sergeev, V.N., Vorob'eva, N.G., Sergeeva, N.D., Selby, D., Johnston, D.T., Knoll, A.H., 2014. Redox heterogeneity of subsurface waters in the Mesoproterozoic ocean. Geobiology 12, 373–386.

Štrok, M., Baya, P.A., Hintelmann, H., 2015. The mercury isotope composition of Arctic coastal seawater. C. R. Geosci. 347, 368–376.

Su, W., Li, H., Huff, W.D., Ettensohn, F.R., Zhang, S., Zhou, H., Wan, Y., 2010. SHRIMP U-Pb dating for a K-bentonite bed in the Tieling Formation, North China. Chin. Sci. Bull. 55, 3312–3323.

Sun, R., Jiskra, M., Amos, H.M., Zhang, Y., Sunderland, E.M., Sonke, J.E., 2019. Modelling the mercury stable isotope distribution of Earth surface reservoirs: implications for global Hg cycling. Geochim. Cosmochim. Acta 246, 156–173.

Tang, D.J., Fu, X.W., Shi, X.Y., Zhou, L.M., Zheng, W., Li, C., Xu, D.T., Zhou, X.Q., Xie, B.Z., Zhu, X.Y., Jiang, G.Q., 2022. Enhanced weathering triggered the transient oxygenation event at similar to 1.57 Ga. Geophys. Res. Lett. 49, e2022GL099018.

Whiteside, J.H., Grice, K., 2016. Biomarker records associated with mass extinction events. Annu. Rev. Earth Planet. Sci. 44, 581–612.

Wu, Y., Yin, R., Li, C., Chen, D., Grasby, S., Li, T., Ji, S., Tian, H., Peng, P., 2022. Global Hg cycle over Ediacaran–Cambrian transition and its implications for environmental and biological evolution. Earth Planet. Sci. Lett. 587, 117551.

Yin, R.S., Krabbenhoft, D.P., Bergquist, B.A., Zheng, W., Lepak, R.F., Hurley, J.P., 2016. Effects of mercury and thallium concentrations on high precision determination of mercury isotopic composition by Neptune Plus multiple collector inductively coupled plasma mass spectrometry. J. Anal. At. Spectrom. 31, 2060–2068.

Zerkle, A.L., Yin, R., Chen, C., Li, X., Izon, G.J., Grasby, S.E., 2020. Anomalous fractionation of mercury isotopes in the Late Archean atmosphere. Nat. Commun. 11, 1–9.

Zhang, K., Zhu, X., Wood, R.A., Shi, Y., Gao, Z., Poulton, S.W., 2018. Oxygenation of the Mesoproterozoic ocean and the evolution of complex eukaryotes. Nat. Geosci. 11, 345–350.

Zhang, S., Wang, X., Wang, H., Bjerrum, C.J., Hammarlund, E.U., Costa, M.M., Connelly, J.N., Zhang, B., Su, J., Canfield, D.E., 2016. Sufficient oxygen for animal respiration 1,400 million years ago. Proc. Natl. Acad. Sci. USA 113, 1731–1736.

Zheng, W., Hintelmann, H., 2010a. Nuclear field shift effect in isotope fractionation of mercury during abiotic reduction in the absence of light. J. Phys. Chem. A 114, 4238–4245.

Zheng, W., Hintelmann, H., 2010b. Isotope fractionation of mercury during its photochemical reduction by low-molecular-weight organic compounds. J. Phys. Chem. A 114, 4246–4253.

Zheng, W., Lin, H., Mann, B.F., Liang, L.Y., Gu, B.H., 2013. Oxidation of dissolved elemental mercury by thiol compounds under anoxic conditions. Environ. Sci. Technol. 47, 12827–12834.

Zheng, W., Gilleaudeaua, G.J., Kah, L.C., Anbar, A.D., 2018. Mercury isotope signatures record photic zone euxinia in the Mesoproterozoic ocean. Proc. Natl. Acad. Sci. USA 115, 10594–10599.